

Artificial neural network potential for gold clusters

Ling-Zhi Cao(曹凌志), Peng-Ju Wang(王鹏举), Lin-Wei Sai(赛琳伟), Jie Fu(付洁), Xiang-Mei Duan(段香梅)

Citation: Chin. Phys. B . 2020, 29(11): 117304 . **doi:** 10.1088/1674-1056/abc15d
Journal homepage: http://cpb.iphy.ac.cn; http://iopscience.iop.org/cpb

What follows is a list of articles you may be interested in

Comparative study on transport properties of N-, P-, and As-doped SiC nanowires: Calculated based on first principles

Ya-Lin Li(李亚林), Pei Gong(龚裴), Xiao-Yong Fang(房晓勇)
Chin. Phys. B . 2020, 29(3): 037304 . **doi:** 10.1088/1674-1056/ab6c4c

Hydrogenated antimonene as quantum spin Hall insulator: A first-principles study

Xin He(贺欣), Ji-Biao Li(李佶彪)
Chin. Phys. B . 2019, 28(3): 037301 . **doi:** 10.1088/1674-1056/28/3/037301

Structural, electronic, and optical properties of hexagonal and triangular SiC NWs with different diameters

Yan-Jing Li(李彦景), Ya-Lin Li(李亚林), Shu-Long Li(李树龙), Pei Gong(龚裴), Xiao-Yong Fang(房晓勇)
Chin. Phys. B . 2017, 26(4): 047309 . **doi:** 10.1088/1674-1056/26/4/047309

Strain-induced insulator-metal transition in ferroelectric $BaTiO_3$ (001) surface: First-principles study

Lin Yang(杨林), Chang-An Wang(王长安), Cong Liu(刘聪), Ming-Hui Qin(秦明辉), Xu-Bing Lu(陆旭兵), Xing-Sen Gao(高兴森), Min Zeng(曾敏), Jun-Ming Liu(刘俊明)
Chin. Phys. B . 2016, 25(7): 077302 . **doi:** 10.1088/1674-1056/25/7/077302

First-principles modeling hydrogenation of bilayered boron nitride

Jing Wang(王静), Peng Zhang(张鹏), Xiang-Mei Duan(段香梅)
Chin. Phys. B . 2016, 25(5): 057301 . **doi:** 10.1088/1674-1056/25/5/057301

SPECIAL TOPIC — Machine learning in condensed matter physics

Artificial neural network potential for gold clusters*

Ling-Zhi Cao(曹凌志)[1,2], Peng-Ju Wang(王鹏举)[3], Lin-Wei Sai(赛琳伟)[4], Jie Fu(付洁)[1,2,†], and Xiang-Mei Duan(段香梅)[1,2,‡]

[1] School of Physical Science and Technology, Ningbo University, Ningbo 315211, China
[2] Laboratory of Clean Energy Storage and Conversion, Ningbo University, Ningbo 315211, China
[3] Key Laboratory of Materials Modification by Laser, Ion and Electron Beams, Ministry of Education, Dalian University of Technology, Dalian 116024, China
[4] College of Science, Hohai University, Changzhou 213022, China

(Received 10 August 2020; revised manuscript received 14 September 2020; accepted manuscript online 15 October 2020)

In cluster science, it is challenging to identify the ground state structures (GSS) of gold (Au) clusters. Among different search approaches, first-principles method based on density functional theory (DFT) is the most reliable one with high precision. However, as the cluster size increases, it requires more expensive computational cost and becomes impracticable. In this paper, we have developed an artificial neural network (ANN) potential for Au clusters, which is trained to the DFT binding energies and forces of 9000 Au_N clusters ($11 \leq N \leq 100$). The root mean square errors of energy and force are 13.4 meV/atom and 0.4 eV/Å, respectively. We demonstrate that the ANN potential has the capacity to differentiate the energy level of Au clusters and their isomers and highlight the need to further improve the accuracy. Given its excellent transferability, we emphasis that ANN potential is a promising tool to breakthrough computational bottleneck of DFT method and effectively accelerate the pre-screening of Au clusters' GSS.

Keywords: empirical potential, artificial neural network, gold cluster, first-principles

PACS: 73.61.At, 34.20.Cf, 84.35.+i, 36.40.–c **DOI:** 10.1088/1674-1056/abc15d

1. Introduction

The unique physical, chemical, and biological properties of clusters in applications such as catalysis, electronics, optics, biosensing, and drug delivery[1–3] have stimulated the increasing interest in cluster science. Extensive research has indicated that the extraordinary behaviors of clusters are originated from the low-coordination edge atoms that lead to a reactive electronic structure as well as absorb binding geometries. This means that the special properties are mainly determined by the ground state structures (GSS) of clusters. However, it is challenging to identify the GSS of clusters either by experimental or theoretical methods, and the research on GSS is a long-standing problem in cluster science.

As a typical cluster, gold (Au) clusters have drawn considerable attention.[4–11] It was reported to have very high catalytic performance in the late 1980s,[12] and the proposal of synthesizing thiol-protected Au clusters method has prompted the researches on Au cluster rapidly.[13–15] With respect to studies on GSS of Au clusters, Oliveira and coauthors probed the stable configurations based on parallel annealing molecular dynamics algorithm,[16] while Dong *et al.* used genetic algorithm.[17] Yet, charges normally alter the structures of neutral Au clusters.[18,19] By now, both theoretical and experimental studies reveal that Au clusters' GSS are remarkably different with cluster size.[20,21] Since most of them have not been identified, and the evolution law with size has not been elucidated, further theoretical and experimental work is required.

First-principles approach based on density functional theory (DFT)[22] is the predominant way to screen cluster GSS in theory. In order to obtain the most stable configuration globally, it is necessary to traverse all possible initial coordinates. However, only from a geometric view, the number of initial coordinates will increase with the size at an exponential rate. The amount of calculations is unbearable for any computers, which makes the DFT method infeasible. Distinct from DFT approach, classical methods are several orders of magnitude faster in the calculation of energy and force. But they turn the problem to find an accurate empirical potential to describe interactions between atoms. So far, several empirical potentials of Au have been reported, such as Sutton–Chen (S–C) potential[23] and Cleri–Rosato potential,[24] which are obtained by fitting to the lattice constants, binding energy, and elastic constants of Au solids. Unfortunately, there is few empirical potential developed for Au clusters.

It should be noted that the traditional empirical potentials are only fitted to some relevant physical properties of Au solids, and the scope of their application in cluster science is very limited. With the development of machine learning

*Project supported by the National Natural Science Foundation of China (Grant Nos. 11804175, 11874033, 11804076, and 91961204) and the K.C. Wong Magna Foundation in Ningbo University.

†Corresponding author. E-mail: fujie@nbu.edu.cn
‡Corresponding author. E-mail: duanxiangmei@nbu.edu.cn

© 2020 Chinese Physical Society and IOP Publishing Ltd

method, artificial neural network (ANN) has become a promising tool in the field of developing empirical potential.[25,26] An ANN architecture designed to describe the atomic interactions is named as ANN potential. It requires few physical models and primarily relies on mathematical expressions and a large number of adjustable parameters in the system. Therefore, ANN potential is an excellent candidate to accurately describe complex high-dimensional first-principles potential energy surfaces[27–31] and be applied in cluster GSS search.

In this work, we are motivated to develop ANN potentials for Au_N clusters with $11 \leq N \leq 100$ atoms by training to DFT binding energy and force via AENET (The Atomic Energy Network)[32,33] software package. The accuracy of the ANN potential is evaluated by testing the energy and force of Au clusters that do not participate in the training as well as clusters reported in literatures. As the results shown, the ANN potential can describe the energy landscape of Au clusters within its error range. In future work, we plan to improve the ANN accuracy and apply it in cluster GSS search.

2. Methods

2.1. Artificial neural network

Artificial neural network is inspired by neuroscience to simulate how does brain process information in biology. In a multilayer perceptron, the input layer accepts input data and propagates to the output layer through several hidden layers. ANN architecture with $n-1$ hidden layers and N_i nodes per layer is represented as N_0–N_1–$\cdots$–N_n (see Fig. 1). The connection between two artificial neurons is described by an analytical form

$$\boldsymbol{x}_{\mathrm{i}}^{(l)} = f^{(l)}\left(\sum_j \boldsymbol{w}_{ij}^{(l)} \boldsymbol{x}_j^{(l-1)}\right) \quad \text{with} \quad l = 1, \ldots, (N-1), \tag{1}$$

where $\boldsymbol{w}_{ij}$ is the weight matrix for transferring signals from layer $l-1$ to layer l, and f is the activation function acting on each parameter vector $\boldsymbol{x}$. In this work, the input data is coordinates of clusters, and the output data is energies and forces on atoms.

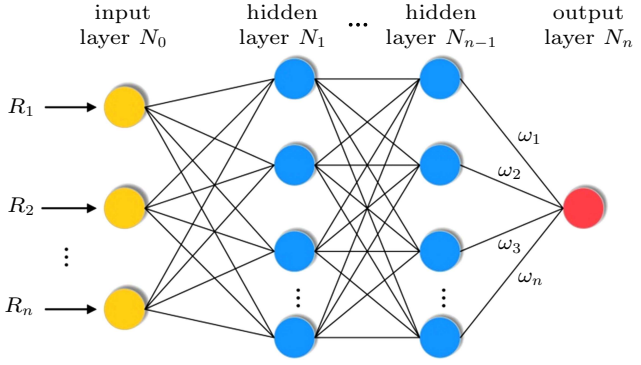


Fig. 1. Schematic diagram of an ANN model (N_0–N_1–$\cdots$–N_n).

2.2. L-BFGS optimization algorithm

ANN potential is trained to DFT binding energy and force data to obtain weight factors of each layer. Algorithm used is the limited memory Broyden–Fletcher–Goldfarb–Shanno (L-BFGS) method. It is a quasi-Newton method based on the second-order expansion of the objective function. The iteration weight parameter $\boldsymbol{w}$ has the form

$$\Delta \boldsymbol{w}^{\mathrm{QN},(I+1)} = -\left(\boldsymbol{H}^{(I)}\right)^{-1} \nabla \xi^{(I)}, \tag{2}$$

where $\boldsymbol{H}$ is an approximation of the Hessian matrix[34–37] and updates at every iteration. Since the L-BFGS method does not store the entire Hessian matrix,[38] it is suitable for ANN training, which has a large number of weight parameters.

2.3. ANN potential

We use Behler and Parrinello[39] type interatomic potential to describe the total energy of a cluster. It sums energy of each atom with the form

$$E(\sigma) = \sum_i^{\text{atoms}} E_i(\sigma) \approx \sum_i^{\text{atoms}} E_i(\sigma_i), \tag{3}$$

where σ is the atomic configuration, and $\sigma_i \subset \sigma$ depends only on coordinates of other atoms locating in range R_{c} centered at atom i. Cartesian coordinate transformation is introduced by an invariant coordinate F with fingerprint function $\tilde{\sigma}_i \equiv F(\sigma_i)$. Therefore, the atomic energy in ANN potential becomes

$$E_i^{\mathrm{ANN}}(\sigma_i) = N[F(\sigma_i)] = N(\tilde{\sigma}_i), \tag{4}$$

where N is a network function. The total energy is approximately equal to the sum of contributions from all atoms

$$E(\sigma) \approx E^{\mathrm{ANN}}(\sigma) \approx \sum_i^{\text{atoms}} E_i^{\mathrm{ANN}}(\sigma_i). \tag{5}$$

The mathematic formulas to describe local structure invariance are a set of basis of radial and angular symmetry functions proposed by Behler and Parrinello (BP).[39–46] They are many-body functions with atomic coordinates in cutoff distance R_{c}. The radial function is defined as

$$G_i^r(\sigma_i) = \sum_{j\neq i}^{\text{neighbors}} g^{\mathrm{r}}(R_{ij}), \tag{6}$$

where $R_{ij} = \left|\boldsymbol{R}_j - \boldsymbol{R}_i\right|$ is the distance between central atom i and adjacent atom j.

Similarly, the angle function depends on three atomic coordinates $\boldsymbol{R}_i$, $\boldsymbol{R}_j$, and $\boldsymbol{R}_k$, and the form is

$$G_i^{\mathrm{a}}(\sigma_i) = \sum_{k\neq j\neq i}^{\text{neighbors}} g^{\mathrm{a}}(\theta_{ijk}),$$
$$\theta_{ijk} = \angle(\boldsymbol{R}_j - \boldsymbol{R}_i, \boldsymbol{R}_k - \boldsymbol{R}_i). \tag{7}$$

The training progress of ANN potential is monitored by the changes of root mean square error (RMSE) and mean absolute error (MAE) of energies and forces on atoms of the reference structures. These two functions are displayed as follows:

$$\mathrm{RMSE} = \sqrt{\frac{1}{N_{\mathrm{tot}}} \sum_{\sigma}^{\text{structures}} \left[E^{\mathrm{ANN}}(\sigma) - E_{\mathrm{ref}}^{\sigma}\right]^2}, \tag{8}$$

$$\mathrm{MAE} = \frac{1}{N_{\mathrm{tot}}} \sum_{\sigma}^{\text{structures}} \left|E^{\mathrm{ANN}}(\sigma) - E_{\mathrm{ref}}^{\sigma}\right|, \tag{9}$$

where N_{tot} is the number of reference structures, $E^{\mathrm{ANN}}(\sigma)$ is the ANN energy of a cluster structure, and $E_{\mathrm{ref}}^{\sigma}$ is the corresponding DFT binding energy.

2.4. First-principles method

The binding energies and forces of the reference cluster structures are obtained via DMol^3 software package[47,48] based on DFT.[49,50] The DMol^3 basis set uses a linear combination of atomic type orbits and Perdew–Burke–Ernzerhof (PBE) exchange correlation functional based on generalized gradient approximation (GGA).[51,52] For the heavy Au element, we use all electron relativistic method to treat the core, and the numerical basis is double numerical plus d-functions (DND). Energy convergence criterion of self-consistent field is set as 1.0^{-4} Ha, while charge and spin density mixing factors are 2.0^{-1} and 5.0^{-1}, respectively. The orbit occupancy is selected by smearing expansion with a spread value 0.005 Ha and the global orbit cutoff is 3.4 Å.

3. Results and discussion

As for training an ANN potential, an important factor in judging whether it is superior is to include as many cluster geometries as possible. Here, in order to make the reference structure diversified, we consider the symmetry of C_1, C_2, C_3, and C_s when generating the structures. Given expensive computational cost of DFT, we randomly generate 25 isomers for each symmetry. Finally, we select 9000 clusters as reference structures among which 90% clusters for training and 10% for test.

Aimed at making ANN energy comparable with DFT binding energy, single atom energy in the ANN potential is set as 0.0 eV. The structure fingerprint of Au clusters is composed of 26 functions with 8 Au–Au radial basis functions and 18 Au–Au angular basis functions. We choose radial basis function of G^2 type and angle basis function of G^4 type.[53] The G^2 type radial basis function of central atom i is defined as

$$G_i^2 = \sum_{j \neq i} \mathrm{e}^{-\eta\left(R_{ij} - R_{\mathrm{s}}\right)^2} \cdot f_{\mathrm{c}}\left(R_{ij}\right), \tag{10}$$

where η is an adjustable parameter. R_{s} is a shift parameter and set as 0 in this work. The smooth cutoff function f_{c} is defined as

$$f_{\mathrm{c}}\left(R_{ij}\right) = \begin{cases} 0.5\left[\cos\left(\dfrac{\pi R_{ij}}{R_{\mathrm{c}}}\right) + 1\right], & \text{for } R_{ij} > R_{\mathrm{c}}, \\ 0, & \text{for } R_{ij} \leq R_{\mathrm{c}}, \end{cases} \tag{11}$$

where R_{c} is the cutoff radius setting as 6.5 Å. The G^4 type angle basis function is defined as

$$\begin{aligned} G_i^4 = {} & 2^{1-\xi} \sum_{j \neq i} \sum_{k \neq i,j} \left(1 + \lambda \cos\theta_{ijk}\right)^{\xi} \cdot \mathrm{e}^{-\eta\left(R_{ij}^2 + R_{ik}^2 + R_{jk}^2\right)} \\ & \times f_{\mathrm{c}}\left(R_{ij}\right) \cdot f_{\mathrm{c}}\left(R_{ik}\right) \cdot f_{\mathrm{c}}\left(R_{jk}\right), \end{aligned} \tag{12}$$

where λ, η, and ζ are adjustable parameters. The parameters used in G^2 and G^4 are shown in the supplementary material.

Table 1. ANN architecture complexity test. Root mean square error (RMSE) and mean absolute error (MAE) are the values after 1000 iterations.

Network architecture	Number of weight parameters	RMSE/(meV/atom)		MAE/(meV/atom)	
		Training set	Test set	Training set	Test set
26–2–2–1	63	19.2	20.4	14.1	14.5
26–5–5–1	171	18.6	17.8	13.7	13.2
26–10–10–1	391	16.2	16.1	12.0	11.9
26–15–15–1	661	16.0	16.7	11.9	12.4
26–20–20–1	981	15.3	17.2	11.4	12.5

Firstly, the effect of the complexity of ANN architecture on the accuracy of ANN potential is examined. As the weight factors become smaller with the increase of hidden layers, normally only 2 hidden layers are adopted, represented as N_0–N_1–N_2–N_3. The number of weight parameters is the sum of connection weights ($N_0 \cdot N_1 + N_1 \cdot N_2 + N_2$) and offset weights ($N_1 + N_2 + 1$). In this work, N_0 is equal to 26, including 8 radial and 18 angle basis functions. The results of complexity test are shown in Table 1. After 1000 iterations, energy RMSE for the training (or test) set of the 26–15–15–1 architecture is 16.0 (or 16.7) meV/atom, and the corresponding MAE is 11.9 (or 12.4) meV/atom. The more complex 26–20–20–1 architecture shows close accuracy to 26–15–15–1. But due to the number of weight parameters increasing dramatically, it will reduce the computational speed of the ANN potential. In contrast, the relatively simple 26–10–10–1 architecture with fewer weight parameters cannot interpolate smoothly in the energy landscape. The discussions indicate that ANN with

2 hidden layers and 15 nodes (26–15–15–1) can achieve the best balance between model accuracy and computational cost. Therefore, we choose the 26–15–15–1 architecture for further research.

To avoid errors caused by overfitting of ANN potential, we assess the number of training iterations required. Generally, overfitting is evaluated by comparing the accuracy of test set to the accuracy of training set. Figure S1 (in the supplementary material) shows that the energy RMSE derivative between training and test sets is 0.1 meV/atom at the 8000$^{\text{th}}$ iteration. Afterwards, the derivative becomes larger, which means overfitting appears. Thus, we choose ANN potential parameters at the 8000$^{\text{th}}$ iteration for further research. Meanwhile, the energy RMSE is 13.4 meV/atom and MAE is 10.0 meV/atom, the force RMSE is 0.4 eV/Å and MAE is 0.4 eV/Å (see Fig. 2).

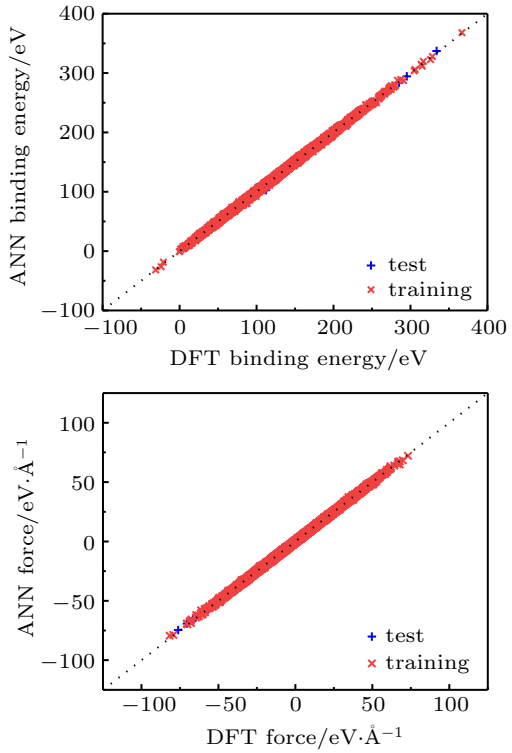


Fig. 2. Comparison of binding energy and force calculated by ANN and DFT.

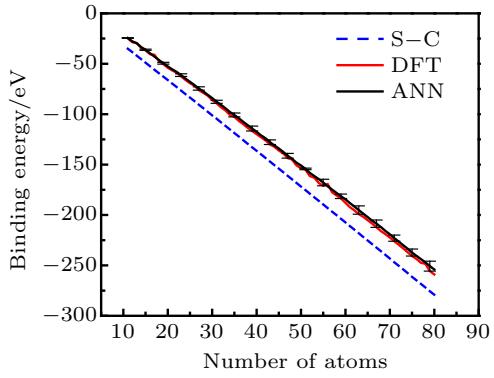


Fig. 3. Calculated binding energies of Au_{11-80} clusters by different approaches.

A good ANN potential can not only accurately calculate the energy of the reference structures, but also the energy of unknown structures. In the following, we move on to test ANN by calculating the binding energy of the most stable Au_{11-80} clusters predicted by S–C potential[54] in the Cambridge Cluster Library.[23,55] As Fig. 3 shown, although the binding energy trends of the S–C and DFT are consistent, while the former is fitted for Au crystal solid, there is a large deviation between the two sets of values. Obviously, the agreement between ANN and DFT is better than that between S–C and DFT. The maximum deviation between ANN and DFT is around 1.8%. The results give much credence to that the ANN potential can accurately describe the binding energy of Au clusters at different sizes.

To figure out how ANN works with isomers at the same size, the cases of Au_{20}, Au_{40}, Au_{60}, and Au_{80} are taken as examples to investigate it (see Fig. 4). We generate 10 cluster isomers randomly at each size and compare their ANN energies to the DFT values. It shows that the ANN potential can reproduce DFT binding energies to a satisfactory extent with maximum error 48.3 meV/atom. The value is greater than ANN energy RMSE. Throughout these 40 isomers, the percentage of clusters with energy error greater than energy RMSE is about 20%, which is statistically reasonable. On the whole, it does not affect the accuracy of the ANN potential to distinguish the energy levels of isomers.

Crucial examination of the ANN potential is facilitated by calculating the binding energies of 12 Au_{27} cluster isomers with the lowest or lower energy reported in the literature.[56] The clusters in Fig. 5 are displayed in the ascending order of DFT binding energy. Taking into account that energy deviations between ANN and DFT are about 1.8 eV, we use relative binding energy $\Delta E = E_i - \bar{E}$ for discussion, where $\overline{E}$ is the average binding energy, and E_i represents the binding energy of the i^{th} isomer. The part where the trends of ANN and DFT are the same is shown in the green area of Fig. 5(b). There are 6 groups of ANN trends consistent with DFT ones and the accuracy ratio is 54.5%. Note that the difference between the maximum and the minimum energy by DFT is about 6.8 meV/atom (see Fig. 5(a)). Therefore, we argue that the inaccuracy is caused by the fact that the DFT energy differences are smaller than the ANN energy RMSE (13.4 meV/atom). It also reveals the disability of ANN potential, that is, it can only deal with the case that the energy difference of clusters is greater than the energy RMSE of ANN potential.

In terms of applications, it is often in trouble for the transferability of a developed empirical potential. Up to date, it is available to recompile ANN package into classic calculation software LAMMPS[57–59] to make the use of the potential more friendly. With the support of various packages from LAMMPS, more calculations about mechanical and thermal

properties (thermodynamics, adsorption, catalyst, transport, etc.) for large size Au clusters will be carried out.

Overall, we build ANN potential for Au clusters, which can accurately describe binding energies of Au clusters within 100 atoms. However, due to the limitation of computational cost by DFT approach, the training set is probably relative small. In this situation, we should pay attention to the energy and force errors of ANN potential for applications.

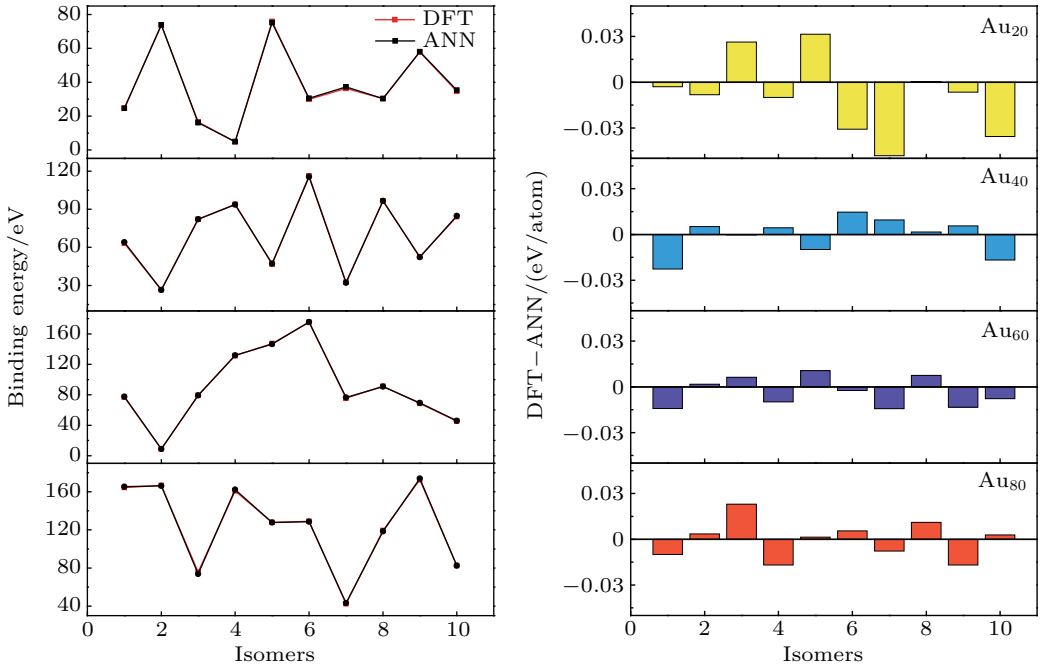


Fig. 4. Comparison of binding energies of Au_{20}, Au_{40}, Au_{60}, and Au_{80} cluster isomers by ANN and DFT.

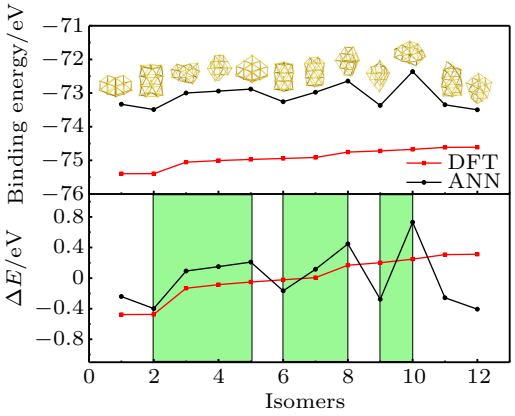


Fig. 5. Binding energies and relative binding energies of Au_{27} isomers by ANN and DFT.

4. Conclusion

With the promising features of machine learning method, we have trained an artificial neural network potential for Au clusters within 100 atoms to DFT data. The ANN potential can be used to describe the binding energy of Au clusters and their isomers with energy error 13.4 meV/atom and force errors 0.4 eV/Å. The development of ANN potential overcomes the bottleneck of expensive computational cost of first-principles methods. Considering its high accuracy as well as efficiency, we plan to combine ANN potential with genetic algorithm to search the ground state structures of Au clusters in our future work.

References

[1] Daniel M C and Astruc D 2004 *Chem. Rev.* **104** 293
[2] Ahmed S, Annu, Ikram S and Yudha S S 2016 *J. Photochem. Photobiol. B* **161** 141
[3] Turkevich J, Stevenson P C and Hillier J 1951 *Discuss. Faraday Soc.* **11** 55
[4] Mingos D M 2015 *Dalton Trans.* **44** 6680
[5] Wang J, Wang G and Zhao J 2002 *Phys Rev B* **66** 035418
[6] Thorn A, Rojas-Nunez J, Hajinazar S, Baltazar S E and Kolmogorov A N 2019 *J. Phys. Chem. C* **123** 30088
[7] Yang D, Pei W, Zhou S, Zhao J, Ding W and Zhu Y 2020 *Angew. Chem. Int. Ed.* **59** 1919
[8] Zhou S, Pei W, Du Q and Zhao J 2019 *Phys. Chem. Chem. Phys.* **21** 10587
[9] Hu Y L, Zhu H R and Wei S H 2019 *Chin. Phys. B* **28** 113101
[10] Du Q, Wu X, Wang P, Wu D, Sai L, King R B, Park S J and Zhao J 2020 *J. Phys. Chem. C* **124** 7449
[11] Chen D D, Kuang X Y, Zhao Y R, Shao P and Li Y F 2011 *Chin. Phys. B* **20** 063601
[12] Haruta M, Yamada. N, Kobayashi T and Iijima S 1989 *J. Catal.* **115** 301
[13] Brust M, Walker M, Bethell D, Schiffrin D J and Whyman R 1994 *J. Chem. Soc., Chem. Commun.* **1994** 801
[14] Mingos D M P 1996 *J. Chem. Soc., Dalton Trans.* **5** 561
[15] Häberlen O D, Chung S C, Stener M and Rösch N 1997 *J. Chem. Phys.* **106** 5189
[16] Oliveira L F L, Tarrat N, Cuny J, Morillo J, Lemoine D, Spiegelman F and Rapacioli M 2016 *J. Phys. Chem. A.* **120** 8469
[17] Dong Y and Springborg M 2007 *J. Phys. Chem. C* **111** 12528
[18] Tarrat N, Rapacioli M, Cuny J, Morillo J, Heully J L and Spiegelman F 2017 *Comput. Theor. Chem.* **1107** 102
[19] Koskinen P, Häkkinen H, Seifert G, Sanna S, Frauenheim T and Moseler M 2006 *New. J. Phys.* **8** 9
[20] Pyykko P 2004 *Angew. Chem. Int. Ed.* **43** 4412
[21] Pyykko P 2008 *Chem. Soc. Rev.* **37** 1967
[22] Xiao L, Tollberg B, Hu X and Wang L 2006 *J. Chem. Phys.* **124** 114309

[23] Sutton A P and Chen J 1990 *Phil. Mag. Lett.* **61** 139
[24] Cleri F and Rosato V V 1993 *Phys Rev B* **48** 22
[25] Artrith N and Kolpak A M 2015 *Comp. Mater. Sci.* **110** 20
[26] Lee K, Yoo D, Jeong W and Han S 2019 *Comput. Phys. Commun.* **242** 95
[27] Sumpter B G and Noid D W 1992 *Chem. Phys. Lett.* **192** 455
[28] Tai No K, Ha Chang B, Yeon Kim S, Shik Jhon M and Scheraga H A 1997 *Chem. Phys. Lett.* **271** 152
[29] Lorenz S, Groß A and Scheffler M 2004 *Chem. Phys. Lett.* **395** 210
[30] Handley C M and Popelier P L 2010 *J. Phys. Chem. A.* **114** 3371
[31] Guo P, Zheng J M, Zhao P, Zheng L L and Ren Z Y 2010 *Chin. Phys. B* **19** 083601
[32] Artrith N and Urban A 2016 *Comp. Mater. Sci.* **114** 135
[33] Artrith N, Urban A and Ceder G 2017 *Phys Rev B* **96** 014112
[34] Broyden C G 1970 *IMA J. Appl. Math.* **6** 76
[35] Fletcher R 1970 *The Computer Journal* **13** 317
[36] Goldfarb D 1970 *Math. Comput.* **24** 23
[37] Shanno D F 1970 *Math. Comput.* **24** 647
[38] Byrd R H, Lu P, Nocedal J and Zhu C 1995 *SIAM. J. Sci. Comput.* **16** 1190
[39] Behler J 2011 *Phys. Chem. Chem. Phys* **13** 17930
[40] Behler J and Parrinello M 2007 *Phys. Rev. Lett.* **98** 146401
[41] Artrith N and Kolpak A M 2014 *Nano. Lett.* **14** 2670
[42] Khaliullin R Z, Eshet H, Kühne T D, Behler J and Parrinello M 2010 *Phys Rev B* **81** 100103
[43] Artrith N, Morawietz T and Behler J 2011 *Phys Rev B* **83** 153101
[44] Morawietz T and Behler J 2013 *J. Phys. Chem. A.* **117** 7356
[45] Artrith N and Behler J 2012 *Phys Rev B* **85** 045439
[46] Artrith N, Hiller B and Behler J 2013 *Phys Status Solidi B* **250** 1191
[47] Delley B 1990 *J. Chem. Phys.* **92** 508
[48] Delley B 2000 *J. Chem. Phys.* **113** 7756
[49] Hohenberg P and Kohn W 1964 *Phys. Rev.* **136** B864
[50] Kohn W and Sham L J 1965 *Phys. Rev.* **140** A1133
[51] Perdew J P, Burke K and Ernzerhof M 1996 *Phys. Rev. Lett.* **77** 3865
[52] Perdew J P, Burke K and Ernzerhof M 1997 *Phys. Rev. Lett.* **78** 1396
[53] Behler J 2011 *J. Chem. Phys.* **134** 074106
[54] Doye J P K and Wales D J 1998 *New. J. Chem.* **22** 733
[55] http://www-wales.ch.cam.ac.uk/CCD.html
[56] Nhat P V, Si N T and Nguyen M T 2020 *J. Phys. Chem. A.* **124** 1289
[57] Plimpton S 1995 *J. Comput. Phys.* **117** 1
[58] G W and Rodrigue G 1989 *Math. Comput.* **53** 775
[59] https://lammps.sandia.gov/